Anal. Chem. **2007,** *79,* 60−70

Time-Resolved pH/pO_2 Mapping with Luminescent Hybrid Sensors

Claudia R. Schröder,[†] Lubos Polerecky,[‡] and Ingo Klimant*[,§]

Institute of Analytical Chemistry, Chemo- and Biosensors, University of Regensburg, 93040 Regensburg, Germany

A method for simultaneous and referenced 2D mapping of pH and pO_2 is described. The experimental setup combines a fast gateable CCD camera as detector, a LED as excitation light source and a single-layer sensor membrane as optical transducer. The planar optode comprises a lipophilic fluorescein derivative (lifetime $\tau \sim 5$ ns) and platinum(II) mesotetrakis(pentafluorophenyl)porphyrin ($\tau \sim 70$ μs in the absence of a quencher) immobilized in a hydrogel matrix. Depending on the fluorescent pH indicator, a pH transition in the physiological range (pH 6−pH 8) or in the near-basic region (pH 7−pH 9) can be achieved. The measuring scheme involves the time-resolved acquisition of images in three windows during a series of square-shaped excitation pulses. A method allowing the calculation of both parameters from these three images is presented. The pH/pO_2 hybrid sensor incorporating the pH indicator 2′,7′-dihexyl-5(6)-*N*-octadecyl-carboxamidofluorescein was characterized in detail. The pH and pO_2 were determined with a maximum deviation of 0.03 pH unit and 6.5 hPa pO_2, respectively, within the range of pH 7.6−pH 8.7 and 0−200 hPa pO_2 in test measurements. The ionic strength (IS) cross-sensitivity was found to be relatively small ($\Delta pH/\Delta IS < 3.5 \times 10^{-4}$ mM^{-1} and $\Delta pO_2/\Delta IS < -0.053$ hPa mM^{-1} at a transition from 0.5 to 0.1 M IS). Whereas a strong temperature effect on the sensor signal was observed ($\Delta pH/\Delta T = 0.011-0.034$ K^{-1} and $\Delta pO_2/\Delta T = 1.85-7.17$ hPa K^{-1} in the range from 277 to 308 K). Examples of pH/pO_2 images obtained in natural marine sediment are presented.

Simultaneous detection of two or more parameters is a field of growing interest in chemical optical sensor development. Multianalyte sensors have been used for the investigation of samples with homogeneous analyte distribution, e.g., in the clinical field for combined measurements of pH, pO_2, and pCO_2 in blood or tissue.[1−4] These sensors incorporate absorbent or luminescent dyes as indicators and can be regarded as an assembly of single-analyte optodes. Since every optode is addressed separately and sensing occurs at different positions, a correlation of the analyte signals in inhomogeneous samples is feasible only if the sensors are sufficiently miniaturized.[5]

The combination of planar optodes and CCD technology led to a significant improvement in high spatial resolution two-dimensional (2D) mapping of single analytes in inhomogeneous samples. This sensor type has been successfully used for gaining insight into 2D distributions and dynamics of pO_2 and pH in marine systems,[6−13] for noninvasive quantification of oxygen supply in engineered tissues,[14] or to visualize airflow patterns in wind tunnel research.[15,16] Since most geochemical, biological, and technical processes involve changes in two or more parameters (e.g., pH, pO_2, pCO_2, Ca^{2+}, glucose, temperature), the information provided by a single-analyte planar optode may be insufficient to understand these processes and their close spatiotemporal coupling. The combination of planar hybrid sensors (based on luminescent indicators immobilized in a single matrix) and the CCD-based imaging technology is therefore a logical step in the development of tools suitable for monitoring of multiple analytes in inhomogeneous systems.

Resolving the signal corresponding to a single analyte from the overall signal of the hybrid sensor becomes increasingly complex with a growing number of target analytes. To date, only

* To whom correspondence should be addressed. E-mail: klimant@tugraz.at. Fax: +43-316-873-4329.

[†] University of Regensburg.

[‡] Current address: Max-Planck Institute for Marine Microbiology, 28359 Bremen, Germany.

[§] Graz Technical University.

(1) Soller, B. R.; Hsi, C.; Favreau, J.; Cingo, N.; Lancey, R. A.; Okike, O. N.; Vander Salm, T. J. *J. Card. Surg.* **2004,** *19*, 167−174.

(2) Venkatesh, B.; Clutton-Brock, T. H.; Hendry, S. P. *J. Cardiothorac. Vasc. Anesth.* **1994,** *9*, 412−419.

(3) Soller, B. R.; Heard, S. O.; Cingo, N. A.; Hsi, C.; Favreau, J.; Khan, T.; Ross, R. R.; Puyana, J. C. *Crit. Care Med.* **2001,** *29*, 1438−1444.

(4) Cooney, C. G.; Towe, B. C.; Eyster, C. R. *Sens. Actuators, B* **2000,** *B69*, 183−188.

(5) Ferguson, J. A.; Healey, B. G.; Bronk, K. S.; Barnard, S. M.; Walt, D. R. *Anal. Chim. Acta* **1997,** *340*, 123−131.

(6) Hulth, S.; Aller, R. C.; Engstrom, P.; Selander, E. *Limnol. Oceanogr.* **2002,** *47*, 212−220.

(7) Zhu, Q.; Aller, R. C.; Fan, Y. *Environ. Sci. Technol.* **2005,** *39,* 8906−8911.

(8) Stahl, H.; Glud, A.; Schroeder, C. R.; Klimant, I.; Tengberg, A.; Glud, R. N. *Limnol. Oceanogr.: Methods,* in press.

(9) Glud, R. N.; Ramsing, N. B.; Gundersen, J. K.; Klimant, I. *Mar. Ecol. Prog. Ser.* **1996,** *140,* 217−226.

(10) Glud, R. N.; Kuehl, M.; Kohls, O.; Ramsing, N. B. *J. Phycol.* **1999,** *35,* 270−279.

(11) Precht, E.; Franke, U.; Polerecky, L.; Huettel, M. *Limnol. Oceanogr.* **2004,** *49,* 693−705.

(12) Polerecky, L.; Franke, U.; Werner, U.; Grunwald, B.; de Beer, D. *Limnol. Oceanogr.: Methods* **2005,** *3,* 75−85.

(13) Franke, U.; Polerecky, L.; Precht, E.; Huettel, M. *Limnol. Oceanogr.* **2006,** *51*, 1084−1096.

(14) Kellner, K.; Liebsch, G.; Klimant, I.; Wolfbeis, O. S.; Blunk, T.; Schulz, M. B.; Goepferich, A. *Biotechnol. Bioeng.* **2002,** *80*, 73−83.

(15) Bell, J. H.; Schairer, E. T.; Hand, L. A.; Mehta, R. D. *Ann. Rev. Fluid Mech.* **2001,** *33,* 155−206.

(16) Engler, R. H.; Klein, C.; Tinks, O. *Meas. Sci. Technol.* **2000**, *11,* 1077−1085.

10.1021/ac0606047 CCC: $37.00
Published on Web 11/24/2006

hybrid sensors for two parameters have been reported. The measuring strategies apply techniques where the signals corresponding to the different analytes are resolved either spectrally (e.g., by using different emission/excitation filters or excitation light sources) or temporally (taking advantage of different decay times of the applied indicators).

Wolfbeis et al. introduced a luminescent pCO_2/pO_2 sensor based on a double-layer design where the signal of each indicator was detected at different wavelengths.[17] A pO_2/temperature hybrid optode was described where a long wave emitting platinum porphyrin and an europium complex were employed as pO_2 and temperature indicators, respectively, and ratiometric intensity measurements with different emission filters were used for quantification of each parameter.[18]

A pCO_2/pO_2 hybrid sensor where both individual sensors contribute to a single optical signal was reported.[19] Frequency domain luminescence phase detection with different modulation frequencies allowed the separation of the oxygen (lifetime) and the carbon dioxide (dual-lifetime referencing, DLR) signals. The advantage of this concept is a very simple and inexpensive optical setup (single light source and detector). A slightly modified concept was used for the signal resolution of a pO_2/temperature fiber-optic hybrid sensor incorporating two phosphorescent indicators. With a multifrequency measurement, it was possible to extract the temperature and the pO_2 information from a rather complex decay behavior of the overall signal.[20,21]

The frequency domain detection schemes are optimally suited for the signal readout from single sensor spots. However, their transfer toward imaging applications requires setups with expensive image intensifiers.[22,23] CMOS-based chips could offer an alternative in the future but are still too insensitive for luminescence-based applications. A feasible alternative is offered by CCD cameras whose image acquisition can be controlled by a rapidly modulated (~100 ns) digital signal. This type of instrumentation enabled the development of referenced imaging methods such as the rapid lifetime determination (RLD)[24−26] and time-domain dual-lifetime referencing (t-DLR)[27] measurement concepts. A hybrid imaging application was reported using a rapidly modulated CCD camera, where a pressure-sensitive paint (PSP) was employed for temperature-corrected imaging of pO_2.[28] The PSP incorporated two phosphorescent indicators with lifetimes in the microsecond (pO_2) and millisecond (temperature) range. Assuming monoexponential decay of both indicators and a constant signal contribution of the long-lived temperature indicator to the fast decaying pO_2 indicator signal, the lifetimes of the dyes were calculated from two sequences of intensity images with increasing time delay from the excitation pulse.

In this work, a novel time-resolved imaging method is presented that combines the RLD and t-DLR techniques into a three-window measuring scheme and allows simultaneous 2D mapping of pH and pO_2. The evaluation method enabling the separation of the signal corresponding to each parameter is presented and its efficiency is investigated. The hybrid sensors applied were optimized with respect to the compatibility of the photophysical properties of the incorporated indicators with available LED technology. In addition, the sensing properties were optimized for the use in marine systems or under physiological conditions. A hybrid sensor incorporating 2′,7′-dihexyl-5(6)-*N*-octadecylcarboxamidofluorescein (DHFA) with a pH transition range in the near-basic region and Pt(PFPP) as an oxygen-sensitive component is characterized in detail, and its stability and cross-sensitivity toward ionic strength and temperature is investigated. As an application example, this hybrid sensor is used for the detection of two-dimensional pH/pO_2 distributions in marine sediment.

EXPERIMENTAL SECTION

Materials. Pt(PFPP) was purchased from Frontier Scientific (Carnforth, UK). 2′-Chloro-7′-hexylfluorescein octadecyl ester (CHFOE) and DHFA were synthesized according to procedures described previously.[29,30] Titanium(IV) oxide (powder, i.d. < 5 μm) was obtained from Aldrich (Taufkirchen, Germany). The polyurethane-type hydrogel HydroMed D4 (D4) was purchased from Cardiotech (Wilmington, MA). The poly(ethylene terephthalate) foil (Mylar, thickness 125 μm) was obtained from Goodfellow (Bad Nauheim, Germany). All buffer salts and organic solvents applied were of analytical grade and were purchased from Merck (Darmstadt, Germany) except for ethanol, which was obtained from Mallinckrodt Baker (Deventer, Netherlands). Doubly distilled water was used throughout. The standard buffer solutions (pH 4 and pH 7) applied for the calibration of the pH meter were purchased from Carl Roth (Karlsruhe, Germany). Phosphate buffer stock solutions with a defined ionic strength (IS) and buffer concentration (15 mM for IS cross-sensitivity measurements, otherwise 50 mM) were prepared with the appropriate sodium salt of dihydrogen phosphate, hydrogen phosphate, or phosphate and with sodium chloride as background electrolyte. If not otherwise stated, the IS of the buffer solutions was adjusted to 500 and 150 mM for measurements with DHFA- and CHFOE-incorporating sensors, respectively. Nitrogen and oxygen (purity >99.9%) as well as synthetic air (20% v/v oxygen in nitrogen) were obtained from Linde (Hoellriegelskreuth, Germany) and were applied to adjust defined oxygen partial pressures during sensor calibration. The sediment and seawater used in the demonstration measurements were from the sand flat Janssand near the island of Spiekeroog, Wadden Sea (North Germany). During the measurements, the seawater was equilibrated with compressed air, which was purchased from Linde.

(17) Wolfbeis, O. S.; Weis, L. J.; Leiner, M. J. P.; Ziegler, W. E. *Anal. Chem.* **1988,** *60*, 2028−2030.
(18) Zelelow, B.; Khalil, G. E.; Phelan, G.; Carlson, B.; Gouterman, M.; Callis, J. B.; Dalton, L. R. *Sens. Actuators, B* **2003,** *B96*, 304−314.
(19) Neurauther G. Ph.D. Thesis, University of Regensburg, 2000.
(20) Stehning, C.; Holst, G. A. *Proc. SPIE* **2002,** *4578*, 259−270.
(21) Stehning, C.; Holst, G. A. *IEEE Sens. J.* **2004,** *4*, 153−159.
(22) Morgan, C. G.; Murray, J. G.; Mitchell, A. C. *Proc. SPIE* **1991,** *1525*, 83−90.
(23) Lakowicz, J. R.; Szmacinski, H.; Nowaczyk, K.; Berndt, K. W.; Johnson, M. *Anal. Biochem.* **1992,** *202,* 316−330.
(24) Holst, G.; Kohls, O.; Klimant, I.; Konig, B.; Kuhl, M.; Richter, T. *Sens. Actuators, B* **1998**, *B51*, 163−170.
(25) Hartmann, P.; Ziegler, W. *Anal. Chem.* **1996,** *68*, 4512−4514.
(26) Liebsch, G.; Klimant, I.; Frank, B.; Holst, G.; Wolfbeis, O. S. *Appl. Spectrosc.* **2000,** *54*, 548−559.
(27) Liebsch, G.; Klimant, I.; Krause, C.; Wolfbeis, O. S. *Anal. Chem.* **2001,** *73*, 4354−4363.
(28) Hradil, J.; Davis, C.; Mongey, K.; McDonagh, C.; MacCraith, B. D. *Meas. Sci. Technol.* **2002,** *13*, 1552−1557.
(29) Weidgans, B. M.; Krause, C.; Klimant, I.; Wolfbeis, O. S. *Analyst (UK)* **2004,** *129*, 645−650.
(30) Schroeder, C. R.; Weidgans, B. M.; Klimant, I. *Analyst (UK)* **2005,** *130*, 907−916.

Table 1. Composition of the Sensor Membranes.

membrane	DHFA/ polymer fraction (mmol kg^{-1})	CHFOE/ polymer fraction (mmol kg^{-1})	Pt(PFPP)/ polymer fraction (mmol kg^{-1})	TiO_2/ polymer fraction (kg kg^{-1})
M_{DHFA}	3	0	0	0
M_{CHFOE}	0	3	0	0
$M_{Pt(PFPP)\_1}$	0	0	6	0
$M_{Pt(PFPP)\_2}$	0	0	6	9/10
$M_{DHFA-Pt(PFPP)}$	3	0	6	9/10
$M_{CHFOE-Pt(PFPP)}$	0	3	3	9/10

Sensor Preparation. A 1-g D4 hydrogel sample was dissolved in 9 g of a 9:1 (v/v) ethanol/water mixture to give a 10% (w/w) stock solution of the sensor matrix polymer. Indicator stock solutions were prepared by dissolving 10 mg of pH indicator in 1 g of ethanol and 15 mg of Pt(PFPP) in 0.5 g of acetone. Aliquots of the dye stock solutions were pipetted to 1 g of the hydrogel solution to make up the final sensor cocktails. Titanium(IV) oxide (TiO_2) powder was added to the sensor solutions of the hybrid sensors and the pure oxygen sensor to enhance light scattering within the sensing layer. The composition of the sensor membranes of the single parameter and hybrid sensors are listed in Table 1. The sensor solutions were stirred for at least 12 h and were afterward spread onto dust-free Mylar foils using a knife-coating device from Coesfeld (Dortmund, Germany) to obtain sensor films with a wet thickness of 60 μm. The membranes were left to dry overnight before measurements and were kept in the dark throughout storage. The sensor membranes were used without preconditioning.

Instrumentation. UV/visible absorbance and transmission spectra were recorded using a U-3000 UV/visible double-beam spectrophotometer from Hitachi (Duesseldorf, Germany). An Aminco Bowman Series 2 luminescence spectrophotometer from SLM-Aminco (Rochester, NY) was used for the acquisition of emission spectra and the calibration curves of the pH membranes M_{CHFOE} and M_{DHFA}. M_{DHFA} was excited at 516 nm, and the fluorescence intensity at 540 nm was recorded. An internally referenced dual excitation scheme was used for M_{CHFOE}. The sensor was excited at 470 and 526 nm, and the fluorescence ratio $F_{\lambda exc526}/F_{\lambda exc470}$ at 545 nm was detected. The setup used for time-resolved imaging (Figure 1A) was described in detail elsewhere.[27,31] It comprises a fast gateable CCD camera (modified SensiCam) from PCO (Kelheim, Germany) with a 0.5-in. monochrome lens-on-chip CCD sensor with 640 × 480 pixels and 12-bit resolution. A custom-made trigger device externally triggers the CCD camera and the light source. The LED array previously used as an excitation light source was replaced by a single LED (Luxeon V Star, lambertian type, λ_{max} = 505 nm from Lumileds (San Jose, CA)). The LED was equipped with a convex lens and a holographic diffuser both from Edmund Industrie Optik (Karlsruhe, Germany) to increase the light field intensity and homogeneity. A combination of a GG 495 long-pass filter and a C54 cyan dichroic short-pass filter was used in the excitation path. The emitted luminescence passed an OG 570 long-pass filter placed in front of the camera lens. All optical filters used were obtained from Schott (GG 495, OG 570, OG590, FITCE; Mainz, Germany) or from Linos Photonics (Dichrolight C54 cyan; Muenchen, Germany). Time-resolved image acquisition was controlled by a computer using a custom-made software module.[31] Image processing was accomplished using an application developed in IDL 5.3 from Research Systems (Boulder, CO). The imaging setup was used for the recording of the calibration curves of the oxygen sensor $M_{Pt(PFPP)\_2}$ applying the RLD scheme[32,33] (see below) and for characterization of the hybrid sensors. The sensor signals R_{pO_2} and R_{pH} were obtained from the ratiometric raw images. Average values of six randomly chosen areas (10 × 10 pixels) in the intensity image ratio were used to calculate the mean value R_x and its standard deviation.

For calibration measurements, the CCD camera and the light source were positioned at the back side of a 5 × 5 cm sensor membrane mounted into a custom-made flow cell (Figure 1B). Buffer solutions with varying pH were equilibrated with nitrogen/oxygen or nitrogen/synthetic air mixtures, respectively, to adjust varying oxygen partial pressures. The pH of the buffer solutions was monitored using a digital pH meter (pH538 multical) with internal temperature compensation from WTW (Weilheim, Germany). Binary gas mixtures were made up using two 1259CC mass flow controllers in combination with a two-channel PR4000 digital power supply and readout from MKS Instruments Deutschland (Muenchen, Germany). The analyte solutions with defined pH and oxygen partial pressure were pumped through a stainless steel tubing into the flow cell by a Miniplus-3 peristaltic pump from Gilson (Villiers-le-Bel, France) connected to the flow cell outlet. The flow rate was kept constant at 1 mL min^{-1} throughout. All measurements were done at 20 °C, if not otherwise stated.

Measurements in a natural marine sediment sample were conducted in accordance to procedures described previously.[8] Pieces of the sensor membrane (1.5 × 5 cm) were fixed to the inner wall of an aquarium made of polycarbonate by a tape (Figure 1C). A thin water-film provided the optical contact between the membrane and the aquarium wall. Afterward, natural surface sediment was added and natural, aerated seawater was let flow slowly above its surface. Temperature was kept constant at 20 °C. After several hours in the dark, a steady-state oxygen gradient between the anoxic sediment and aerated water developed and several sets of pH/pO_2 images were acquired. pH and pO_2 profiles were additionally measured using microelectrodes.[34,35]

RESULTS AND DISCUSSION

Membrane Design. The composition of a hybrid sensor should ideally ensure that the signals for the single-target analytes are not influenced by the other analyte or by an interaction between the two indicators. Moreover, in the presented 2D sensing scheme, a constant intensity ratio of the two luminophores within the sensing area is important since otherwise varying pH values are simulated. For this work, it was decided to use single-layer membranes with the two indicator dyes dissolved in the polyurethane-based matrix polymer. The beneficial aspects of this concept are the straightforwardness of the sensor preparation and the high homogeneity of the sensor films with a uniform molecular

(31) Holst, G.; Grunwald, B. *Sens. Actuators, B* **2001,** *74,* 78−90.
(32) Woods, R. J.; Scypinski, S.; Cline Love, L. J.; Asworth, H. A. *Anal. Chem.* **1984,** *56,* 1395−1400.
(33) Ballew, R. M.; Demas, J. N. *Anal. Chem.* **1989,** *61,* 30−33.
(34) Revsbech, N. P. *Limnol. Oceanogr.* **1989,** *34,* 474−478.
(35) Revsbech, N. P.; Jorgensen, B. B. *Adv. Microbiol. Ecol.* **1986,** *9,* 293−352.

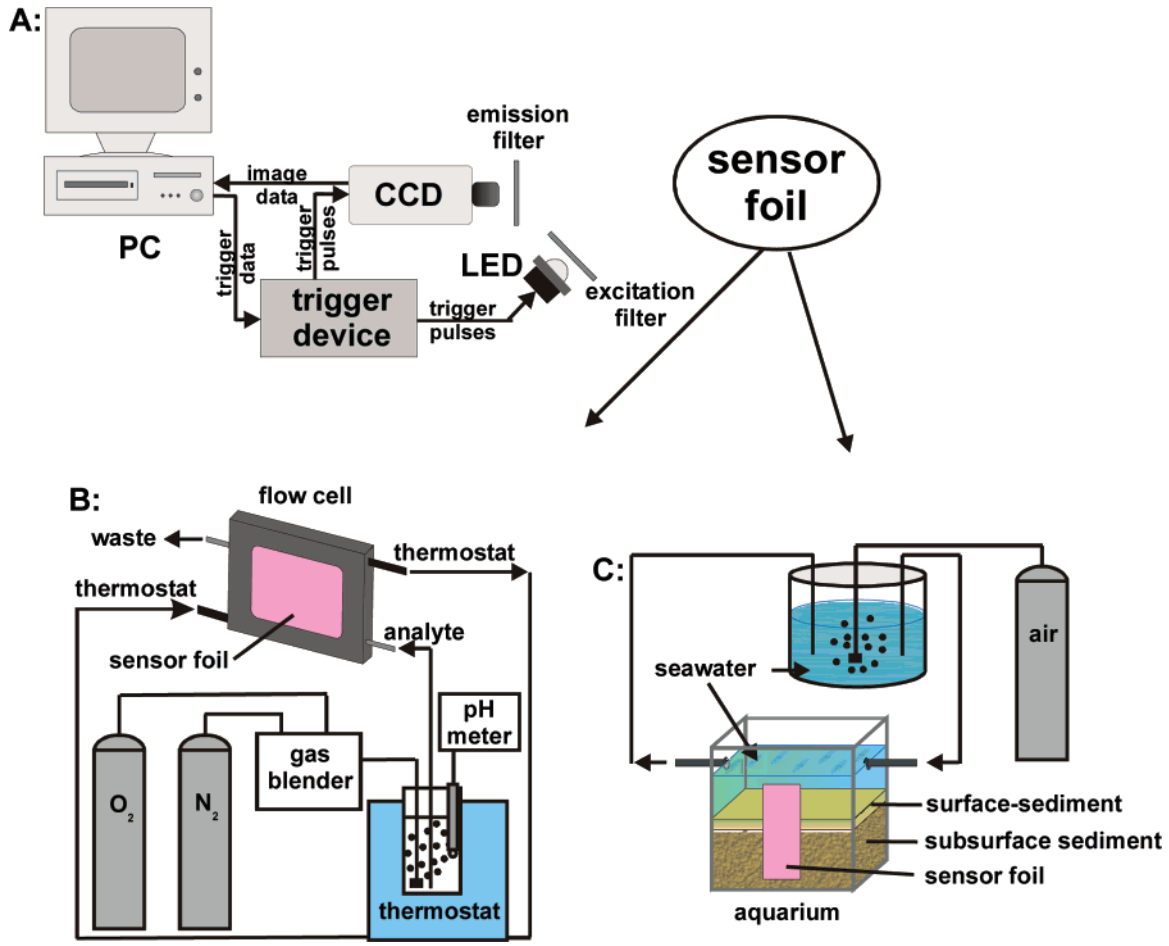

Figure 1. Schematic of the imaging setup (A) and the experimental setup used for the sensor characterization (B) and for the measurement in marine sediment (C).

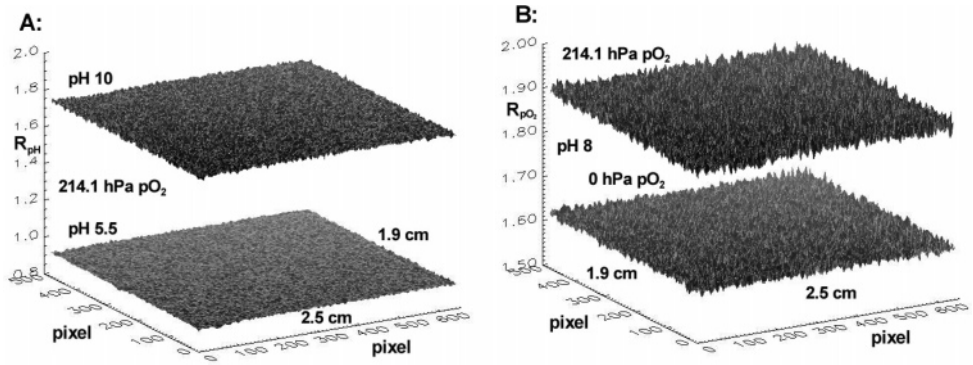

Figure 2. Uncorrected images (2.5 × 1.9 cm areas) of the $M_{DHFA-Pt(PFPP)}$ sensing membrane; (A) t-DLR−pH measurement (R_{pH}) taken at pH 5.5 and 10 (pO_2 = 214.1 hPa); (B) RLD−oxygen measurement (R_{pO_2}) taken at 0 and 214.1 hPa pO_2 (pH 8).

distribution of both dyes, as demonstrated by the raw sensor images R_{pH} and R_{pO_2} (Figure 2). However, possible effects such as resonance energy transfer (RET), inner filter effects, or increased photobleaching due to highly reactive singlet oxygen formed during the collisional quenching process between oxygen and the oxygen indicator were not evaded by this approach and were therefore characterized in detail below.

Choice of Indicators. Spectral Properties. An important criterion for the choice of a pH and pO_2 indicator combination was the possibility to apply one single-excitation light source and the same optical filters for both dyes. The fluorescent pH indicators considered for the use in hybrid sensors were the two lipophilic fluorescein derivatives DHFA and CHFOE.[29,30] They were combined with the phosphorescent oxygen-sensitive indicator Pt(PFPP). The uncharged, highly proton-permeable hydrogel Hydromed D4 served as the sensor matrix. It contains hydrophilic regions and hydrophobic blocks in which the pH indicators with their alkyl side chains are immobilized by adsorption. The protonated DHFA exists predominantly as a nonfluorescent lactone due to the lipophilic surrounding within polymer matrix. The absorbance and emission maximums of the deprotonated DHFA are at 516 and 540 nm, respectively. An esterification of the 2-carboxyl group in the fluorescein chromophore such as in CHFOE prevents the lactonization of the dye at low pH values.

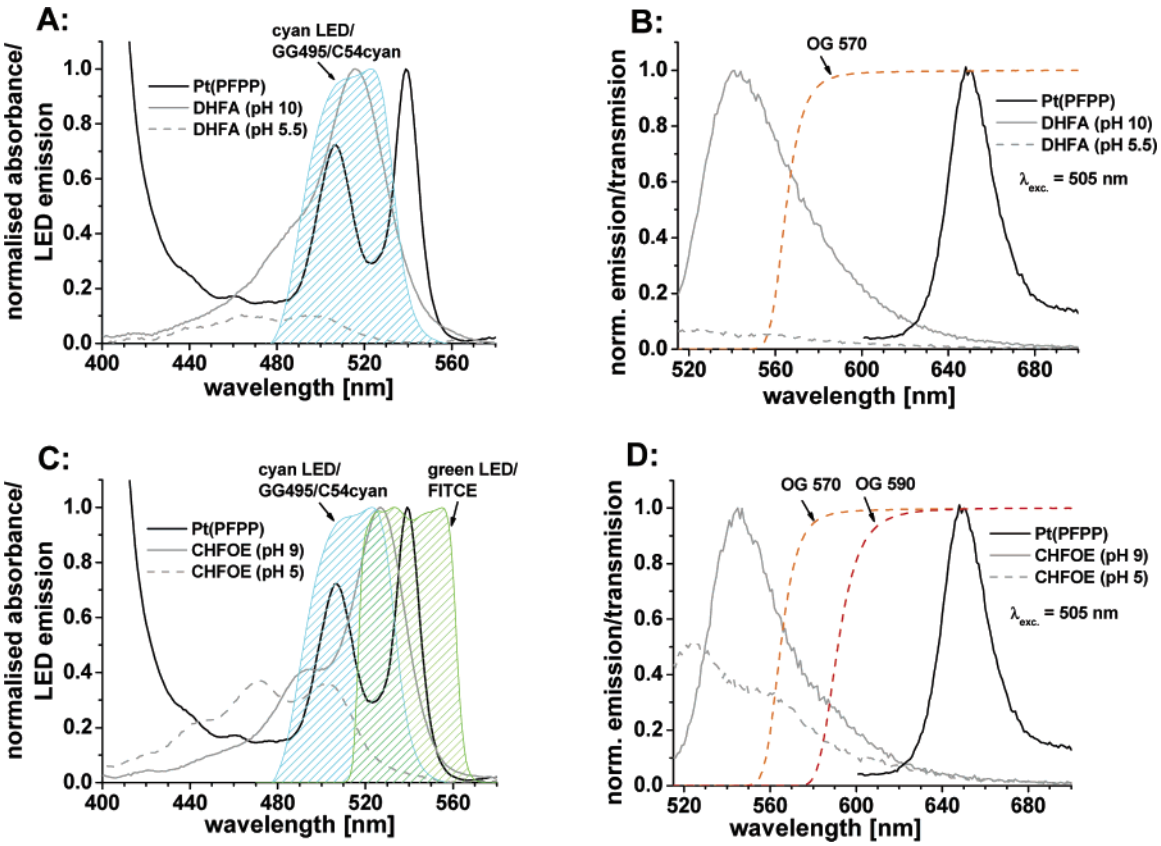

Figure 3. Normalized absorbance (A, C) and luminescence (B, D) spectra of the indicators applied in the hybrid sensors $M_{DHFA-Pt(PFPP)}$ (A, B) and $M_{CHFOE-Pt(PFPP)}$ (C, D). The spectra were recorded with indicators immobilized in D4 membranes (M_{CHFOE}, M_{DHFA}, and $M_{Pt(PFPP)\_1}$ (see Table 1)); emission spectra of suitable light sources combined with the transmission spectra of the necessary filter sets as well as the transmission spectra of the emission filters are also shown.

Hence, the protonated form of the ester is also fluorescent. The absorbance/emission maximums of the protonated and deprotonated forms of CHFOE are at 470/523 and 526/545 nm, respectively. Pt(PFPP) embedded in D4 shows an emission maximum at 648 nm and absorbance maximums at 391 (Soret band), 507, and 539 nm. The latter two are in the same wavelength region as the absorbance maximums of the deprotonated fluoresceins, which allows the usage of low-cost excitation light sources such as LEDs or xenon lamps.

The 505-nm emitting LED equipped with the filter combination GG495/C54 cyan is ideally suited for simultaneous excitation of both indicators in the DHFA/Pt(PFPP) hybrid sensor (Figure 3A). The OG570 long-pass emission filter is needed to remove any LED stray light. Although only a small part of the emission of the deprotonated DHFA is recorded, the sensor dynamics toward pH is still high since the protonated form of DHFA is not fluorescent (Figure 3B). The same LED and filter combination were used for the CHFOE/Pt(PFPP) hybrid sensor although it was not optimal, as the protonated form of CHFOE is also excited by the 505-nm LED (Figure 3C). Therefore, the sensor dynamics of the pH sensor is reduced, since the fluorescence emission of the protonated CHFOE is relatively high within the detected wavelength region. An alternative approach, comprising the 530-nm LED and the FITCE filter for excitation, was not pursued, because it would require the usage of the OG590 emission filter, which would lead to a strong decrease of the detected fluorescence from the pH indicator (Figure 3D).

Characteristics of the Single-Parameter Sensors. Figure 4A shows the calibration curves of the pH membranes M_{DHFA} and M_{CHFOE}. The normalized fluorescence (M_{DHFA}) and the normalized fluorescence ratio (M_{CHFOE}) were plotted against pH, respectively, and fitted by the Boltzmann (sigmoidal) function

$$\frac{F}{F^0} = \frac{m1 - m2}{1 + \exp\left(\frac{\mathrm{pH} - \mathrm{p}K_a'}{p}\right)} + m2 \qquad (1)$$

where F and F^0 are the fluorescence (ratio) signals measured at varying pH values and at the highest pH value used during the calibration (M_{CHFOE}, pH 9; M_{DHFA}, pH 10), respectively. The parameters $m1$, $m2$, pK_a', and p are empirical parameters describing the initial value ($m1$), the final value ($m2$), the point of inflection (pK_a'), and the width (p) of the sigmoidal curve. The points of inflection corresponding to the apparent pK_a values (pK_a') were at 7.13 and 8.35 for M_{CHFOE} and M_{DHFA}, respectively. Thus, pH sensors incorporating CHFOE cover the important pH range for physiological applications (e.g., in medicine and biotechnology), while hexyl substituents in 2′- and 7′-position of DHFA shift the dynamic range of the sensor to the near-basic region, which is ideal for pH measurements in marine environment.

The calibration curves of the oxygen sensor $M_{Pt(PFPP)\_2}$ are depicted in Figure 4B. The lifetimes τ were calculated from the sensor signal R_{pO_2} as

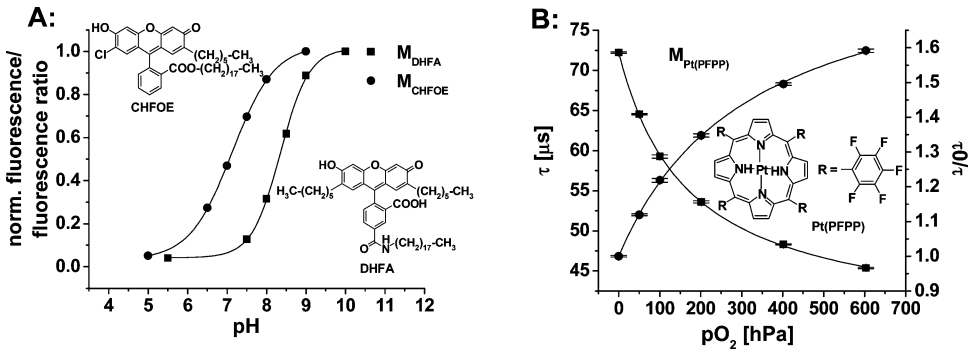

Figure 4. Calibration curves of the pure pH sensors M_{DHFA} and M_{CHFOE} (A) and the pure oxygen sensor $M_{Pt(PFPP)}$ (B). The calibration of $M_{Pt(PFPP)\_2}$ was accomplished with phosphate buffer solutions at pH 7 equilibrated with various oxygen partial pressures.

$$\tau = \frac{t_2 - t_1}{\mathrm{Ln}(R_{\mathrm{pO_2}})} \quad \text{with} \quad R_{\mathrm{pO_2}} = A_{\mathrm{em1}}/A_{\mathrm{em2}} \qquad (2)$$

where A_{em1} and A_{em2} are the intensity integrals obtained from the first and second intensity images taken after the excitation pulse, respectively, and t_2 and t_1 are the time delays between the end of the excitation pulse and the start of the recording of the corresponding image. The resulting lifetimes are weighted mean lifetimes since the assumption of a monoexponential decay cannot be made for the indicator embedded in a polymer matrix. These weighted mean lifetimes τ and the ratio $\tau 0/\tau$ were plotted against pO_2 and fitted by the modified Stern−Volmer equation based on two-site quenching model[36,37]

$$\frac{\tau 0}{\tau} = \left[\frac{f}{1 + K_{\mathrm{sv}}\mathrm{pO_2}} + (1 - f)\right]^{-1} \qquad (3)$$

where $\tau 0$ and τ are the lifetime of Pt(PFPP) in the absence and presence of oxygen, respectively. K_{sv} is the Stern−Volmer constant, which contains the bimolecular quenching constant of the dynamic quenching reaction, f and $(1 - f)$ represent the quenchable and nonquenchable fractions of the luminescence, respectively. This two-site quenching model does not reflect the true conditions in the sensor matrix (the decay behavior of the indicator molecules within the hydrogel is multiexponential rather than two-exponential). However, eq 2 was suitable to fit the oxygen calibration curve with a minimum of fitting parameters. The following fitting parameters and correlation coefficient R^2 were found: $\tau 0 = 72.3 \pm 0.2\ \mu s$, $f = 0.474 \pm 0.005$, $K_{sv} = (5.95 \pm 0.18) \times 10^{-3}\ \mathrm{hPa^{-1}}$, and $R^2 = 0.9998$. The sensitivity of Pt(PFPP) in D4 toward oxygen is quite low, which makes the sensor applicable over a wide pO_2 range. Although this is at the cost of the sensor resolution at small pO_2 values, a better resolution is obtained for oxygen partial pressures between 200 and 600 hPa.

Characterization of the DHFA/Pt(PFPP) Hybrid Sensor. Spectral Interactions between the Two Indicator Dyes. The $M_{DHFA-Pt(PFPP)}$ sensor membrane was immersed in phosphate buffer solutions at pH 10 and pH 5.5 and equilibrated either with nitrogen (0 hPa pO_2) or air (216.8 hPa pO_2). The recorded luminescence intensity spectra (Figure 5) show that the phosphorescence intensity of Pt(PFPP) is influenced by pH. The intensity of the band at 648 nm significantly decreases at the transition from the N_2/pH 10 buffer to the N_2/pH 5.5 buffer, where it is even slightly lower than that detected with the air/pH 10 buffer. Both emission bands of DHFA at pH 10 (N_2 and air) show an intensity decrease in the wavelength range between 534 and 547 nm. This intensity loss at selective wavelengths indicates an inner filter effect, which is promoted by the TiO_2 particles dispersed in the membrane. This is due to an overlap of the absorbance band of Pt(PFPP) at 539 nm and the emission band of DHFA in this range of the spectrum, which also enables RET from DHFA to Pt(PFPP).

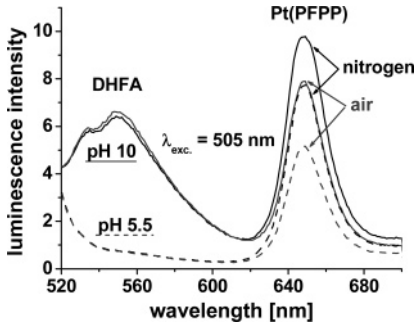

Figure 5. Luminescence spectra of $M_{DHFA-Pt(PFPP)}$ measured with buffer solutions at pH 10 (solid lines) and pH 5.5 (dashed lines) equilibrated with nitrogen and air.

t-DLR/RLD Hybrid Measuring Scheme. The measuring scheme applied for time-resolved imaging with the pH/pO_2 hybrid sensors combines the two-window based RLD and t-DLR measuring schemes into a single, three-window-based hybrid scheme (Figure 6). It enables the recording of the signals for both parameters during one measuring sequence. The first intensity image is recorded during the excitation pulse (Δt_{ex} = 35 or 50 μs) and contains the luminescence emission of both indicators A_{pH} and A_{pO_2} (the parameter A stands for an intensity integral not an area). The second and third images comprising the intensity integrals A_{em1} and A_{em2} are recorded after the excitation pulse ($\Delta t_{em1} = \Delta t_{em2} = 35\ \mu s$). Recording starts a short time delay (200 ns) after the end of the excitation pulse, during which any short-lived fluorescence is decayed. Consequently, the images contain only the phosphorescence emission of the oxygen indicator.

The oxygen signal R_{pO_2} is then given by the intensity integral ratio A_{em1}/A_{em2} accordingly to the RLD method. This ratio is independent of the distribution of the excitation light field and the distribution of the indicator within the sensing membrane and

(36) Carraway, E. R.; Demas, J. N.; DeGraff, B. A. *Anal. Chem.* **1991,** *63,* 332−336.

(37) Carraway, E. R.; Demas, J. N.; DeGraff, B. A.; Bacon, J. R. *Anal. Chem.* **1991,** *63,* 337−342.

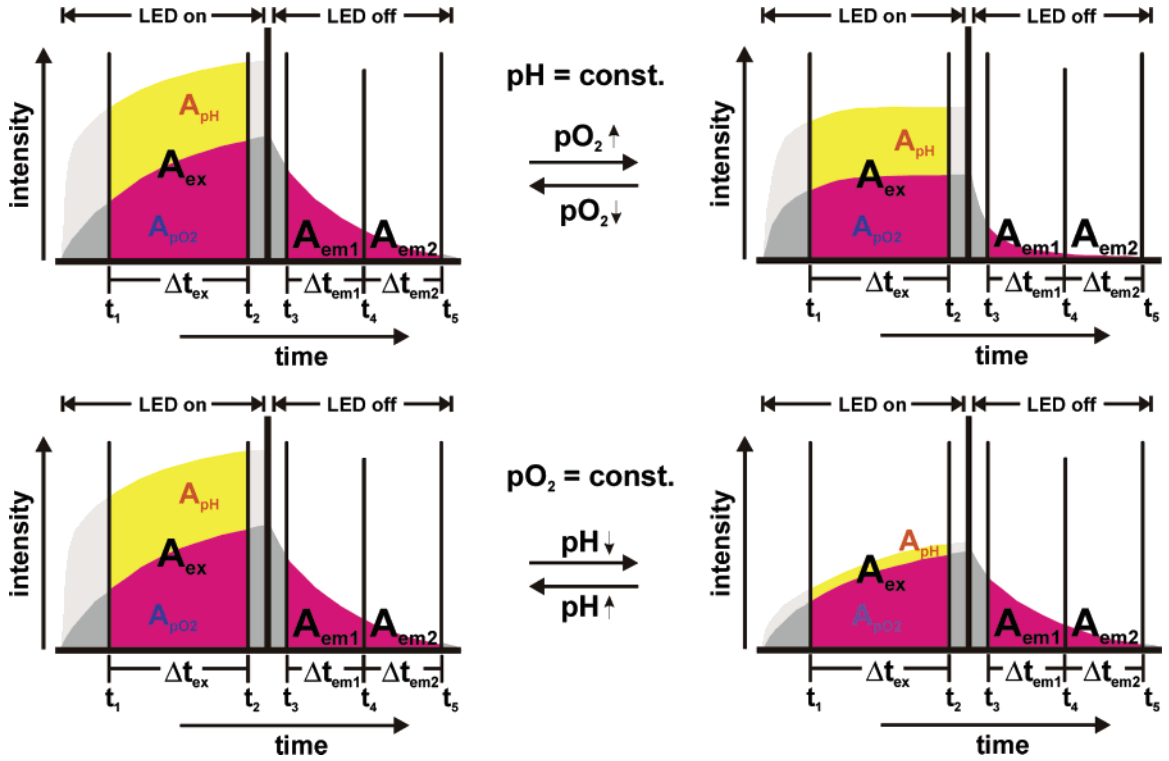

Figure 6. Schematics of the three-window t-DLR/RLD hybrid scheme used for the simultaneous mapping of pH and pO_2. The fluorescence intensity of the pH indicator reaches saturation within a few nanoseconds after the start of the excitation pulse and is depicted as a constant offset to the increasing phosphorescence intensity (μs lifetime) of the oxygen indicator during the excitation period (50-μs duration).

does not change if the indicator leaches or undergoes photodecomposition. Information about pH is carried by the intensity integral ratio $R_{pH} = A_{ex}/(A_{em1} + A_{em2})$ and is independent of the absolute intensity from a single pixel. However, a homogeneous distribution of the two indicators is important, since a change in the proportion of the dyes simulates variations in pH. Furthermore, intensity losses due to leaching or photobleaching of one or both luminophores are not referenced out in this scheme.

Since the signal of the pH indicator A_{pH} is not referenced with the constant signal of an inert, long-lived reference dye (as is done in the original t-DLR scheme), but with the oxygen-dependent signal of the second indicator, R_{pH} is a function of both pH and pO_2 (eq 4)

$$R_{pH}(pH, pO_2) = \frac{A_{pH}}{(A_{em1} + A_{em2})} + \frac{A_{pO_2}}{(A_{em1} + A_{em2})} \quad (4)$$

where A_{pH} and A_{pO_2} are the luminescence intensity integrals of the pH and oxygen indicators during excitation and A_{em1} and A_{em2} are the phosphorescence intensity integrals of the oxygen indicator after the excitation phase, respectively. Thus, a two-dimensional calibration function describing the behavior of R_{pH} over the relevant range of pH and pO_2 is required to enable the recovery of pH and pO_2 of an unknown sample from the measured R_{pH} and R_{pO_2} values. The pO_2 of the sample is determined by means of the R_{pO_2} versus pO_2 calibration function, and the pH is afterward calculated with this pO_2 from the $R_{pH}(pH, pO_2)$ function.

Equation 4 can be separated into pH-dependent and oxygen-dependent parts. The fluorescence intensity of the pH indicator reaches saturation within a few nanoseconds after the onset of the excitation pulse (50-μs duration). It can, therefore, be assumed to be time-independent and A_{pH} can be expressed in the form of a Boltzmann equation (compare eq 1). The pO_2 influence on R_{pH} is due to the oxygen dependence of A_{pO_2} and $(A_{em1} + A_{em2})$ (Figure 6). Introducing the Boltzmann equation and two oxygen-dependent functions $C_1(pO_2) = A_{pO_2}/(A_{em1} + A_{em2})$ and $C_2(pO_2) = (A_{em1} + A_{em2})^{-1}$ into eq 4, R_{pH} can be written as

$$R_{pH}(pH, PO_2) = C_2(pO_2)\left(\frac{m1 - m2}{1 + \exp\left(\frac{pH - pK_a'}{p}\right)} + M2\right) + C_1 \quad (pO_2) \quad (5)$$

Equation 5 was used to fit the calibration plots of R_{pH} versus pH measured for the $M_{DHFA-Pt(PFPP)}$ sensor (Figure 7A). In the first step, the calibration plot measured at $pO_2 = 0$ hPa was fitted with the parameters m_2, pK_a', p, and C_1 being variable and the parameters C_2 and m_1 being fixed to 1 and 0, respectively. Fixing C_2 at $pO_2 = 0$ hPa to 1 corresponds to a arbitrary normalization, which at the same time implies that A_{pH} is referenced by this constant factor. In the subsequent steps, m_1 and the values for m_2, pK_a', and p found in the first step were fixed and only C_1 and C_2 were varied to fit the R_{pH} versus pH calibration plots at the other oxygen partial pressures. The correlation coefficients R^2 of the R_{pH} versus pH fits were always higher than 0.9984. The values of C_1 and C_2 found by this fitting procedure were plotted against pO_2 and fitted with second-order polynomials (data not shown). Introduction of $C_1(pO_2)$, $C_2(pO_2)$ and the Boltzmann fit parameters into eq 5 leads to the required two-dimensional $R_{pH}(pH, pO_2)$ function. The corrected R_{pH} versus pH calibration plots show that

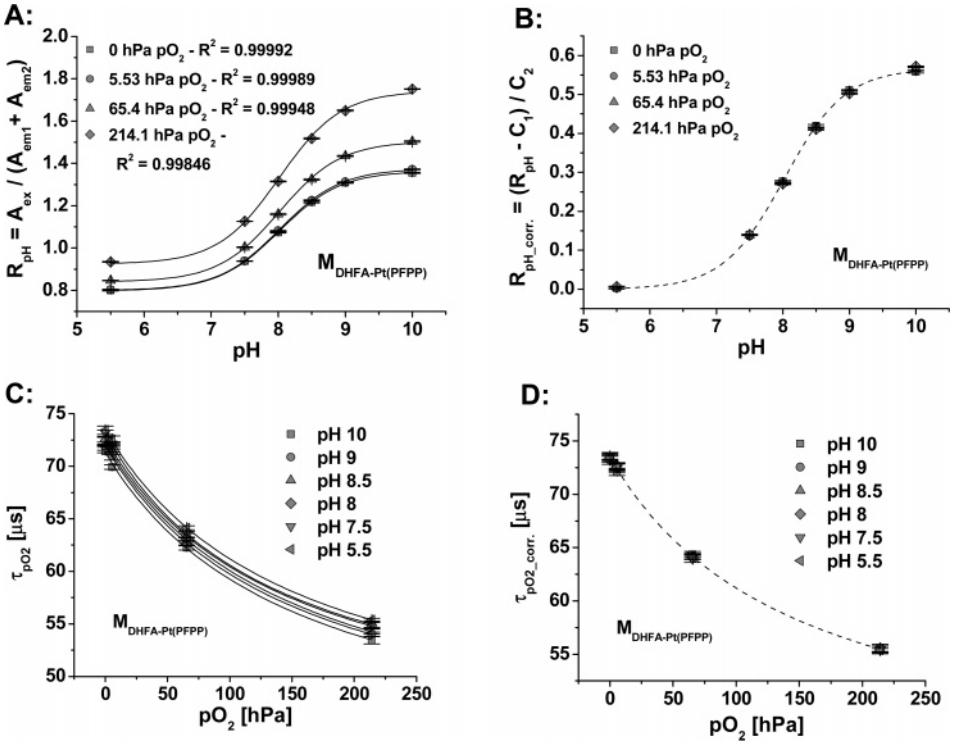

Figure 7. Uncorrected and corrected R_{pH} versus pH (A, B) and τ_{pO_2} versus pO_2 (C, D) calibration curves of $M_{DHFA-Pt(PFPP)}$.

Table 2. Standard Deviations of the Corrected pH (σpH).

	σpH		
	0 hPa pO_2	65.4 hPa pO_2	214.1 hPa pO_2
pH 9	±0.17	±0.24	±0.41
pH 8.5	±0.08	±0.11	±0.19
pH 8	±0.04	±0.06	±0.13
pH 7.5	±0.02	±0.06	±0.14

after correction all calibration points lie on the Boltzmann function found in the fitting procedure (Figure 7B).

Standard deviations of the pH value caused by the errors in the measured R_{pH} values and the parameters obtained in the fitting procedure were calculated for various positions in the R_{pH}(pH, pO_2) plane (Table 2).

As shown in the hybrid measuring scheme, the detection of the oxygen signal R_{pO_2} is not influenced by the fluorescence of the pH indicator (Figure 6). However, the R_{pO_2} and therefore the calibration plots of the uncorrected values of τ_{pO_2} calculated from eq 2 clearly display a cross-sensitivity toward pH of the buffer solution (Figure 7C). We think that this is due to the pH-dependent water uptake capacity of the hydrogel sensor matrix, where the nonpolar oxygen indicator molecules are localized in the hydrophobic areas. Examination of the parameters of the Stern−Volmer calibration functions (eq 3) used to fit the uncorrected τ_{pO_2} versus pO_2 plots revealed that mainly $\tau 0$ depends on pH, while the pH effect on f and K_{sv} was less significant. Since the $\tau 0$ value is not influenced by the oxygen permeability of the polymer, its pH-dependent change was contributed to the altered polarity in the vicinity of Pt(PFPP) while the pH-dependent change of the K_{sv} value containing the bimolecular quenching constant was contributed to an altered oxygen permeability.

A relatively simple correction of the τ_{pO_2} calibration curves for the pH dependence is possible. Average offsets from the calibration curve at pH 5.5 were calculated as $\Delta\tau_{pO_2\_mean}(pH) = \tau_{pO_2}(pH) - \tau_{pO_2}(pH\ 5.5)$ and fitted with a Boltzmann function (data not shown). Hence, the pH-independent pO_2 calibration function $\tau_{pO_2\_corr.}$ can be determined as

$$\tau_{pO_2\_}\mathrm{corr.}(pO_2) = \frac{t_4 - t_3}{\mathrm{Ln}(R_{pO_2}(pH, pO_2))} + \Delta\tau_{pO_2\_}\mathrm{mean}(pH) \quad (6)$$

where t_3 and t_4 are the time delays between the end of the excitation pulse and the start of the recording of the corresponding image (see Figure 6). The mean $\tau_{pO_2\_corr.}$ values of the corrected τ_{pO_2} calibration plots were fitted by a Stern−Volmer function (Figure 7D). Substitution of $\tau_{pO_2\_corr.}(pO_2)$ in eq 6 by this mean Stern−Volmer function gives the two-dimensional equation, which describes R_{pO_2} as a function of pH and pO_2.

$$R_{pO_2}(pH, pO_2) = \exp\left(\frac{t_4 - t_3}{\tau 0\left[\frac{f}{1 + K_{sv}pO_2} + (1 - f)\right] - \Delta\tau_{pO_2\_}\mathrm{mean}\ (pH)}\right) \quad (7)$$

Iteration Procedure. Since R_{pH} and R_{pO_2} depend on both pH and pO_2, an iterative evaluation is necessary to determine pH and pO_2 of an unknown sample from the set of calibration curves characterizing the hybrid sensor. In the first step, the two-dimensional calibration functions R_{pH}(pH, pO_2) (eq 5) and R_{pO_2} (pH, pO_2) (eq 7) were resolved for the pH and the pO_2, respectively. Subsequently, pH 8 was selected as the pH starting

Table 3. pH and pO_2 Values Calculated Iteratively from the R_{pH} and R_{pO_2} Values Measured by the $M_{DHFA-Pt(PFPP)}$ Sensor in Five Test Buffer Solutions.

	calculated pH/pO_2 values									
	S1 (pH 9.2/ 91.2 hPa pO_2)		S2 (pH 8.7/ 121.6 hPa pO_2)		S3 (pH 8.2/ 60.8 hPa pO_2)		S4 (pH 7.6/ 20.3 hPa pO_2)		S5 (pH 6.5/ 202.6 hPa pO_2)	
iteration step	pH	pO_2 (hPa)	pH	pO_2 (hPa)	pH	pO_2 (hPa)	pH	pO_2 (hPa)	pH	pO_2 (hPa)
0	8.0	103.7	8.0	128.1	8.0	64.4	8.0	20.9	8.0	193.0
1	8.91	98.2	8.67	123.4	8.22	63.3	7.6	22.3	6.72	200.2
2	9.00	97.7	8.72	123.1	8.23	63.2	7.59	22.3	6.62	200.4
3	9.01	97.6	8.72	123.1	8.23	63.2	7.59	22.3	6.61	200.4

value and was inserted into R_{pO_2}(pH, pO_2) together with the measured R_{pO_2} to calculate an initial pO_2 value. This pO_2 value was used together with the measured R_{pH} and R_{pH}(pH, pO_2) to determine a new pH value. The iteration procedure was repeated until the difference of the pO_2 values of the actual and the previous iteration step was less than 0.05 hPa. Then the pO_2 value was used to calculate the final pH. This iteration procedure was tested with five buffer solutions (S1−S5) and with a $M_{DHFA-Pt(PFPP)}$ sensor calibrated according to the procedures described above. Table 3 lists the pH and pO_2 values adjusted in the test buffer solutions and those calculated by the iteration procedure in three iteration steps. The results show that already after the first iteration step the pO_2 values can be assumed to be constant within the precision of measurement, due to the small pH dependence of the oxygen signal (Figure 7C). As a consequence, final pH values are obtained in the second iteration step. The deviation between the calculated and the adjusted pH values increases at the upper and lower boundary of the dynamic range of the hybrid sensor, inducing also a stronger deviation of the determined pO_2 values (see S1).

Sensor Stability. Leaching and Photodecomposition of the Indicators. The leaching of the indicators from the membrane was tested with a phosphate buffer solution adjusted to pH 8.2 (IS = 500 mM) and saturated with ambient air. A $M_{DHFA-Pt(PFPP)}$ sensor was mounted into the flow cell and calibrated. Subsequently, the pH 8.2 buffer solution was pumped through the cell and images were taken after 2, 4, 6, and 24 h. Between the measurements, the cell was kept in the dark. The measured R_{pH} values were converted into apparent pH values using the calibration function, and the detected deviations from the set pH 8.2 were plotted against time. After a strong decrease of the apparent pH of −0.14 within the first 2 h, the apparent pH decreased at a constant rate of $\Delta pH/\Delta t = -0.0031\ h^{-1}$ (data not shown). The leaching of the oxygen indicator was less pronounced. Within the investigated time of 24 h, $A_{em1} + A_{em2}$ decreased to 98.6% of the initial value. The strong signal change at the beginning of the measurement due to an increased leaching of the pH indicator suggests a preconditioning of the sensor membrane. After this period, however, the pH error caused by indicator leaching is comparatively small.

A more serious problem is the indicator loss due to photodecomposition. While the oxygen indicator has an increased photostability because of the fluoro substituents of the porphyrin ligand, fluoresceins and especially the dihexyl derivative DHFA are less stable.[30,38] To investigate the photodecomposition of the indicators, the hybrid sensor was first calibrated in the flow cell with buffer solutions of the same composition as used in the leaching experiment. After calibration of the sensor membrane, the measuring cell was filled with the pH 8.2 buffer solution and a series of 100 measurements were made. During each measurement, the membrane was exposed to 6250 excitation pulses (50-μs duration) with an irradiance of ∼5.1 mW/cm^2, which corresponds to the total exposure of ∼1.6 mJ/cm^2. The decrease of the apparent pH was approximately linear and amounted to $\Delta pH = -0.002$ per measurement, while $A_{em1} + A_{em2}$ decreased by 0.015% per measurement.

Cross-Sensitivity toward Ionic Strength. The effect of the IS on the sensor signal is a well-known problem in optical pH sensing.[39] This cross-sensitivity originates from the fact that the proton activity of the sample is detected via the change in an optical property (e.g., absorbance, fluorescence intensity) and, therefore, a concentration change of the protonated or deprotonated pH indicator, or both. Thus, the activity coefficients of the two indicator species and the solvent activity are not taken into account. Changes in these factors, however, shift the measured signal and simulate a different pH. The IS cross-sensitivity of the pure pH sensors with the indicators DHFA and CHFOE in D4 was described previously.[29,30] While the IS effect on the CHFOE sensor was negligible, the DHFA-containing sensor displayed a stronger cross-sensitivity due to the additional negative charge of the 2-carboxyl group at high pH values. The effect of IS on the corrected pH calibration curves of the $M_{DHFA-Pt(PFPP)}$ membrane is small at IS values higher than 300 mM (Figure 8A). The maximum deviation in the measured pH (Δ_{max}pH) in the pH range from 7.5 to 9 at a transition from 500 to 300 mM is 0.05, which is within the measurement precision. At a transition to lower IS values, however, the cross-sensitivity becomes more pronounced (Table 4).

The corrected pO_2 calibration curves also depend on IS (Figure 8B). The sensitivity of the sensor toward pO_2 slightly increases with decreasing IS. The influence of the IS was quantified by using the $\tau_{pO_2\_corr.}$ values at varying IS and at 0, 100, 210, 300, and 400 hPa pO_2 to calculate apparent pO_2 values from the calibration curve at 500 mM IS. The obtained apparent pO_2 values were plotted against the IS and linear regression gave the $\Delta pO_2/\Delta IS$ gradients, which are summarized in Table 4.

Temperature Effect. Variations in temperature have an impact on the signal of both indictors in $M_{DHFA-Pt(PFPP)}$. The deactivation of the excited state is enhanced at increasing temperatures due

(38) Lee, S.-K.; Okura, I. *Anal. Commun.* **1997,** *34,* 185−188.

(39) Janata, J. *Anal. Chem.* **1987,** *9,* 1351−1356.

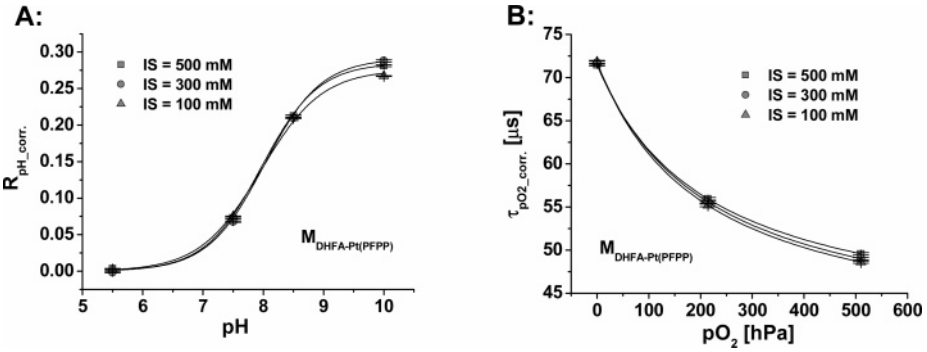

Figure 8. Corrected pH (A) and pO_2 (B) calibration curves of $M_{DHFA-Pt(PFPP)}$ measured with phosphate buffer solutions adjusted to IS values varying from 100 to 500 mM.

Table 4. Influence of IS and Temperature on the Apparent pH and pO_2 Measured with the $M_{DHFA-Pt(PFPP)}$ Hybrid Sensor.

pH	ΔpH_{max} (IS: from 500 to 100 mM)	pH	$\Delta pH/\Delta T$ (K^{-1}) at $pO_2 = 0$ hPa	$\Delta pH/\Delta T$ (K^{-1}) at $pO_2 = 210$ hPa	pO_2 (hPa)	$\Delta pO_2/\Delta IS$ (hPa mM^{-1})	$\Delta pO_2/\Delta T$ (hPa K^{-1})
7.5	0.02	7.2	0.008	0.024	0	0.0057	1.85
8	0.03	7.6	0.011	0.028	100	−0.017	4.11
8.5	0.09	7.8	0.014	0.029	210	−0.053	7.17
9	0.19	8	0.017	0.034	300	−0.09	9.89
		8.2	0.022	0.037	400	−0.142	13.12

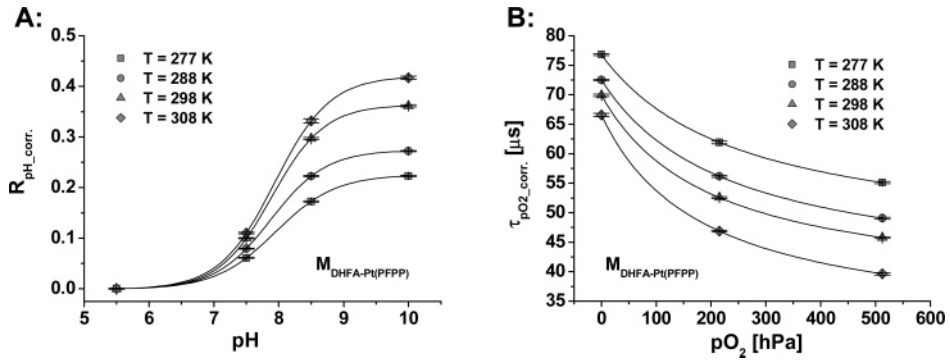

Figure 9. Corrected pH (A) and pO_2 calibration curves (B) of $M_{DHFA-Pt(PFPP)}$ recorded at temperatures from 277 to 308 K. cboth display a strong temperature cross-sensitivity.

to internal and external conversion. In the case of DHFA, there is also an influence on the equilibrium constant of the acid−base reaction. Previous measurements with the pure pH sensor in the temperature range from 277 to 308 K showed that these two effects compensate over a wide pH range for DHFA in D4, so that the temperature cross-sensitivity is negligible up to pH 8.5.[30]

The corrected pH and pO_2 calibration curves of $M_{DHFA-Pt(PFPP)}$ both depend strongly on temperature (Figure 9). The contrast between the large temperature dependence of the pH part of the hybrid sensor and that of the pure pH sensor is due to the fact that the hybrid sensor pH signal A_{pH} is referenced with the constant factor $C_2(pO_2 = 0$ hPa) originating from the highly temperature-dependent pO_2 indicator luminescence. This is the predominant effect on the corrected pH signal and leads to increasing $R_{pH\_corr.}$ values at increasing temperature. The influence of the temperature on the measured pH and pO_2 was quantified by applying the calibration curves at 298 K to calculate apparent pH and pO_2 values from the measured values at other temperatures. Table 4 shows the $\Delta pO_2/\Delta T$ and $\Delta pH/\Delta T$ gradients found by linear regression. $\Delta pH/\Delta T$ gradients were calculated for two different oxygen partial pressures exemplarily, due to the strong temperature influence on the $C_1(pO_2)$ and $C_2(pO_2)$ functions.

pH and pO_2 Imaging in Natural Marine Sediment. As a proof of principle, the $M_{DHFA-Pt(PFPP)}$ hybrid sensor was applied for the mapping of pH and pO_2 in marine sandy sediment. The raw data of the images of the sediment measurements were used to calculate the pH and pO_2 distribution over the entire area of the sensor membrane according to the iteration procedure described above. Figure 10A depicts examples of false color images of the pH and pO_2 distributions. Vertical profiles extracted from these images (white lines in the maps) as well as the profiles obtained using microelectrodes are displayed in Figure 10B.

CONCLUSION

A novel measuring scheme was successfully applied for the simultaneous, referenced pH and pO_2 imaging with planar, optical hybrid sensors. In principle, this scheme allows the detection of the pH signal as a hybrid signal dependent on pH and pO_2 and the pO_2 signal as a pure signal only dependent on pO_2. A generally applicable procedure to generate a two-dimensional function

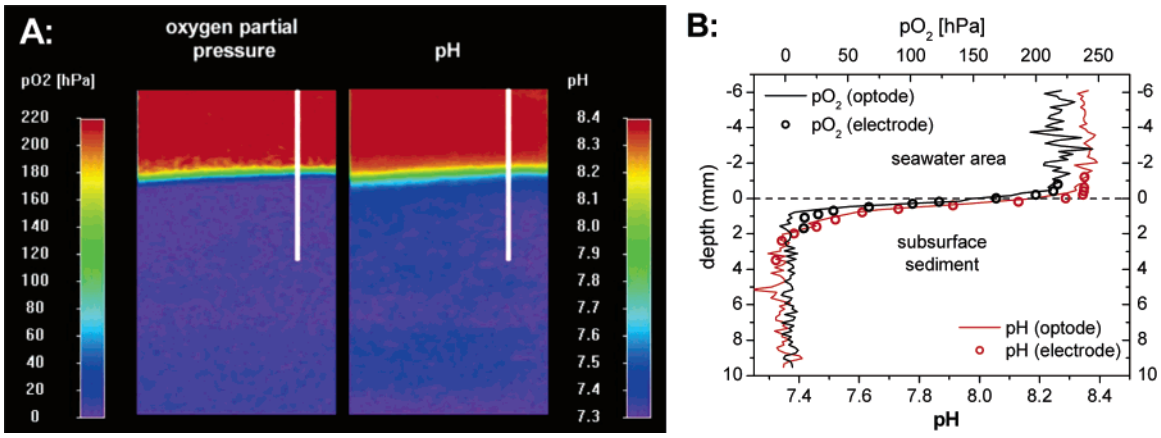

Figure 10. False color maps of the pH and pO_2 (A) distributions in natural marine sediment; profiles extracted from the maps as well as profiles measured with microelectrodes (B).

describing the pH signal in dependence of pH and pO_2 is also described. The planar optical hybrid sensors were fabricated by dissolving the two indicators in a single-layer polymer matrix. The benefits are the straightforwardness of the procedure and the homogeneity of the resulting sensor membranes, but consequences are also a reduced long-term stability and an influence of pH on the measured pO_2 signal, due to pH-dependent polarity of the sensor polymer. Therefore, an iteration procedure is necessary to calculate the pH and pO_2 values from the measured raw data of the hybrid sensors presented in this work. Measurements with five test buffer solutions using a DHFA- and Pt(PFPP)-containing hybrid membrane gave a maximum deviation of 0.03 pH unit and 6.5 hPa pO_2 within the range of pH 7.6−pH 8.7 and 0−200 hPa pO_2. However, standard deviations between ±0.02 and ±0.19 pH unit were calculated for the corrected pH values. Thus, the benefit of the simultaneous detection of pH and pO_2 is at the cost of a decreased precision compared to the respective single parameter sensors, where usually a pH sensor precision of ±0.03 pH unit and a pO_2 sensor precision of ±2 hPa is achieved. A high leaching rate of the pH indicator was detected within the first 2 h, which is not referenced by the measuring scheme and causes a shift of the apparent pH by ∼0.14 pH unit. Thus, the sensor foils should be preconditioned before measurements. After this time, errors due to leaching are low but still can become considerable in long-term measurements. Long-term use of the sensors also suffers from problems related to photobleaching, affecting especially the pH signal. The IS cross-sensitivity of the pH part of the hybrid sensor is comparable to that of the pure pH sensor. A slight sensitivity increase of the pO_2 sensor part at decreasing IS was observed. The temperature influence on the signals of both parameters, however, is comparably high. Thus, a parallel temperature control is inevitable. To limit measurement errors, a calibration of the hybrid sensor at the temperature and IS of the sample is preferable to a subsequent correction. The application of the DHFA/Pt(PFPP) hybrid sensor in natural marine sediment gave the expected trends in the pH and pO_2 distribution. However, minimization of the photodecomposition effects on the membrane long-term performance is vital to make the hybrid sensor useful in quantitative studies, especially if they involve illumination by light over extended time periods. That can be achieved by using an optically isolated sensor layer, which in addition also excludes possibly interfering background fluorescence of the sample. This, however, requires further development of the sensor composition. Due to the possibility to replace DHFA by a pH indicator with a dynamic range in the physiological region (CHFOE), this sensing system can be extended to further application fields, such as noninvasive monitoring of transcutaneous pO_2 and pH, or measuring of pO_2 and pH imaging in biofilm research.

ACKNOWLEDGMENT

This work was supported by the Bundesministerium fuer Bildung und Forschung (BMBF) Project 03F02848.

Received for review April 1, 2006. Accepted September 12, 2006.

AC0606047